Methodology for the assessment of equivalent load for self-lubricating radial spherical plain bearings under combined load

AUTHOR #1: Josu Aguirrebeitia, PhD.
Associate Professor.
Department of Mechanical Engineering.
ETSI-BILBAO. University of the Basque Country.
Alameda de Urquijo, s/n, 48013 BILBAO, SPAIN.
E-mail: josu.aguirrebeitia@ehu.eus

AUTHOR #2: Mikel Abasolo, PhD (corresponding author).
Assistant Professor.
Department of Mechanical Engineering.
EUITI-BILBAO. University of the Basque Country.
Alameda de Urquijo, s/n, 48013 BILBAO, SPAIN.
E-mail: mikel.abasolo@ehu.eus

AUTHOR #3: Javier Vallejo, PhD.
Associate Professor.
Department of Mechanical Engineering.
ETSI-BILBAO. University of the Basque Country.
Alameda de Urquijo, s/n, 48013 BILBAO, SPAIN.
E-mail: javier.vallejo@ehu.eus

AUTHOR #4: Ibai Coria, MSc.
Department of Mechanical Engineering.
ETSI-BILBAO. University of the Basque Country.
Alameda de Urquijo, s/n, 48013 BILBAO, SPAIN.
E-mail: ibaicoriamartinez@gmail.com

AUTHOR #5: Iker Heras, MSc.
Department of Mechanical Engineering.
ETSI-BILBAO. University of the Basque Country.
Alameda de Urquijo, s/n, 48013 BILBAO, SPAIN.
E-mail: iker.heras @ehu.eus

ABSTRACT

This work presents a model to assess the equivalent load for self-lubricating radial spherical plain bearings under combined loads, based on the study of the interference field. Using an algorithm based on the model, a methodology has been created to estimate failure load combinations. The results, validated via Finite Element Analysis, are presented in the form of load magnification factors for equivalent load assessment, which prove to be similar to those provided by manufacturer catalogues. The contribution of this work lies in explaining the technical background of these factors, not explained in any catalogue or standard, further developing a methodology that will enable any manufacturer to generate the values for their particular products and design parameters.

Keywords: Spherical plain bearing, conformal contact, load capacity, methodology.

1. Introduction

Spherical plain bearings are suitable for applications where mating parts work under large angular misalignments, encompassing sectors as material handling, mining, railways, wind energy… Fig. 1 shows the different types of spherical plain bearings: radial, axial and angular contact. Radial bearings are designed to carry radial load, but they can simultaneously accommodate a certain magnitude of axial load; on the contrary, axial bearings are used for predominantly axial loads, but they can also carry radial loads; finally, angular contact bearings are suitable for load combinations where axial and radial components are of the same magnitude. The present work centers on radial spherical plain bearings.

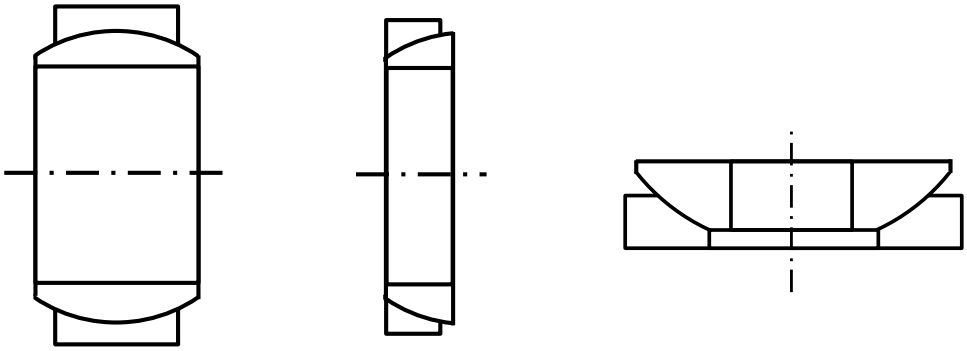

Fig. 1. Spherical plain bearing types: (a) radial (b) angular contact (c) axial

The dimensions of the radial spherical plain bearings are standardized [1,2]; they are designed with a radial internal clearance Δr, defined as the distance through which one of the rings may be displaced relative to the other, from one eccentric position to the diametrically opposite extreme position, whose minimum and maximum values are also normalized. Bearing may or not require maintenance: for steel/steel or steel/bronze contacts, the bearing must be greased prior to being put into operation and it must be relubricated periodically (lubrication holes and grooves are provided for such purpose). In

maintenance-free bearings contact surface is steel/PTFE, which is self-lubricating, so they operate without grease and relubrication, even though occasional relubrication in some cases it can extend the service life of the bearing. The present work focuses on maintenance-free or self-lubricating radial spherical plain bearings.

Regarding the loads acting on the bearing, they are considered static if there is no continuous relative movement between the rings and dynamic otherwise. Radial static load capacity represents the maximum radial load which the bearing can withstand without inadmissible deformations, fracture or damage to the sliding contact surfaces, whereas radial dynamic load capacity is the maximum radial load which the bearing can carry without excessive wear under certain operating conditions.

Even though a draft standard is now being prepared by the ISO/TC4/SC8/WG8, currently there is no standardized formula for the calculation of the load capacity; in this sense, manufacturers compute it as the product of a specific load factor and the effective projected sliding surface.

Nevertheless, as it has been mentioned, radial spherical plain bearings can accommodate radial and axial load combinations; for F_a and F_r load combinations, manufacturers propose calculating an equivalent radial load P to be compared with the load capacity C_r (static or dynamic) to determine if failure will occur:

$$P = Y \cdot F_r < C_r \tag{1}$$

In equation (1), Y is the load magnification factor, which depends on the ratio of the axial to the radial load F_a/F_r. Thus, the load magnification factor implicitly defines the failure load combinations. Fig. 2 shows the diagram with its values for self-lubricating radial spherical plain bearings of manufacturer SKF [3]. There are two curves: one for series GEP..FS, and the other one for the other series.

Failure of a spherical bearing occurs when the maximum contact pressure reaches a limiting value, but manufacturers do not explain how the pressure distribution is calculated, and thus the background of their load magnification factors is unknown. Due to the conformity of spherical plain bearings, the contact area is large relative to the size of the rings, so Hertz treatment does not estimate the pressure distribution accurately [4-6]. Other analytical models were also proposed by Steuermann and Goodman, which proved to be limited to small contact angles or large clearances [5, 7-8]. More recently, numerical models have been used to formulate pressure distribution [9-11]. Fang et al. proposed a semi-analytical and semi-numerical model, adjusted and validated via FEA, for the estimation of the pressure distribution in complete [10] and incomplete [11] spherical contacts. Laszlofalvi et al. published in the SKF Ball Bearing Journal a model that estimates the interference field and pressure distribution in a simplified way, replacing the real spherical surface by a cylindrical surface for radial loads [12]. In reference [13], Laszlofalvi et al. generalized the model to estimate the pressure distribution under combined axial and radial forces, approximating the contact surface by tapered surfaces. In this sense, the latter is the only work currently published that deals with combined loads in spherical plain bearings. However, replacing the real contact surface by approximated ones involves a loss of accuracy; besides, the model enables to calculate the maximum contact pressure under a given load combination, in order to verify whether its magnitude is below

the design limiting value to determine if the selected bearing is valid, but no procedure to obtain the load magnification factors is explained.

The present work develops a model to calculate the magnification factors of self-lubricating radial spherical plain bearings. The model by Laszlofalvi et al. is improved by studying the interference field using the real spherical contact surface; the approach proposed in the present work is more rigorous, and therefore provides more accurate results. This is not the first time the authors have applied successfully a geometric interference model to account for pressure distribution in other machine elements: in [14] the generalized load capacity of rolling bearings was addressed showing a good finite element correlation, and in [15] the circumferential pressure distribution was experimentally correlated for lip seals in reciprocating motion as a function of the rod-to-bore eccentricity. Then, as a straightforward and generalist application, a procedure has been created in this work to calculate the load magnification factors for self-lubricating radial spherical plain bearings by means of this proposed model. The obtained factors have been compared with the ones provided by SKF and with Finite Element results.

It must be remarked in this point that interference field, and not deformation field, is used to account for pressure distribution. In this sense, it is known that a rigorous way to solve the pressure distribution would need a consistent study of the deformation field, as in [10,11]. However, the aim of this work was to obtain a simple and inexpensive model to estimate the pressure distribution, and for such purpose the authors believe that the interference field approach appears to be more convenient.

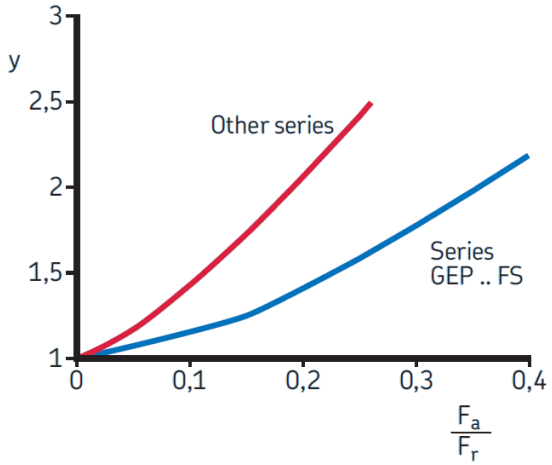

Fig. 2. Fa/Fr-Y curves for SKF self-lubricating radial spherical plain bearings [3].

2. Proposed model

The new semi-analytical model developed in this work imposes a displacement to the inner ring, keeping the outer ring fixed. This generates an interference field in the contact surface, which in turn causes a pressure distribution. The radial and axial loads are calculated by integration of the pressure field over the contact area. Next, this calculation process is explained. For the sake of simplicity, first a pure radial load case will be

analyzed, and afterwards the procedure will be generalized for a radial and axial combined load case.

2.1 Pure radial load case

Once the inner and outer rings are in contact after having overcome the internal clearance $\Delta r/2$ between them, the inner ring is displaced a distance δ_0 following a displacement line with radial direction as shown in Fig. 3 (spherical coordinates $\theta=\psi=0$). This displacement is caused by a radial load F_r, whose value wants to be calculated. From Fig. 4 the extension of the interference (expressed as a fraction ε of the contact diameter d) is extracted as a function of δ_0 and Δr [12]:

$$\left.\begin{aligned} {}^{d}/_{2}\cdot cos\beta &= \left({}^{d}/_{2}-{}^{\Delta r}/_{2}\right)\cdot cos\alpha \\ sin\beta &= \frac{{}^{d}/_{2}-\varepsilon\cdot d}{{}^{d}/_{2}} \\ sin\alpha &= \frac{{}^{d}/_{2}-\varepsilon\cdot d-{}^{\Delta r}/_{2}-\delta_0}{{}^{d}/_{2}-{}^{\Delta r}/_{2}} \end{aligned}\right\} \rightarrow \varepsilon = \frac{\delta_0}{\Delta r+2\cdot\delta_0} \tag{2}$$

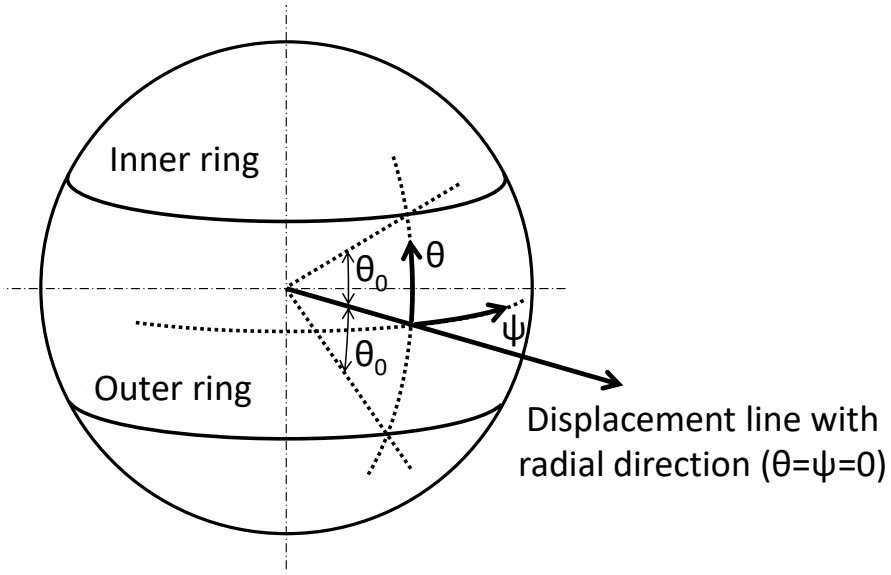

Fig. 3. Displacement line with radial direction ($\theta=\psi=0$).

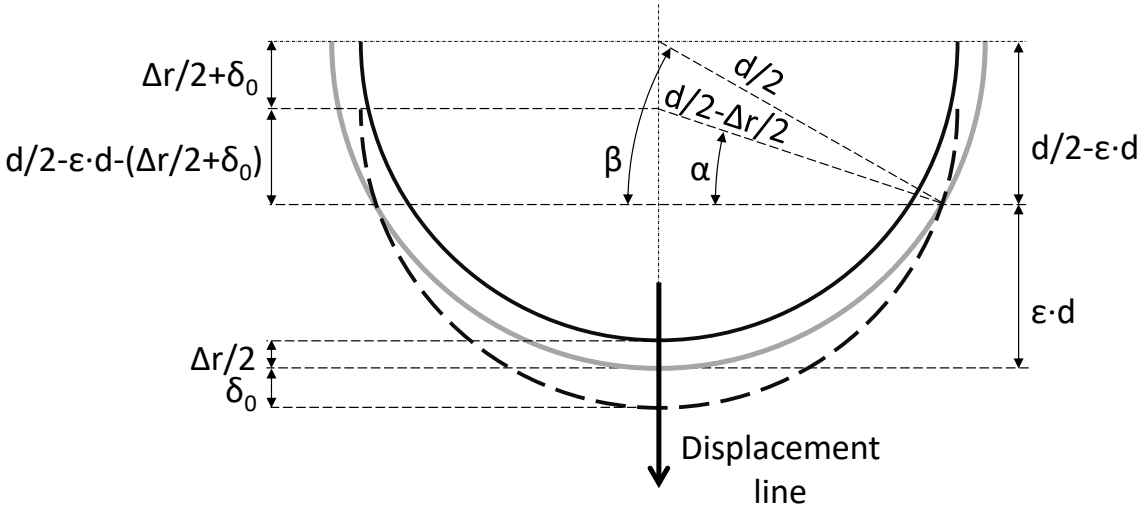

Fig. 4. Graphical representation of the extension of the interference ε·d.

Next, the interference field in the contact surface between the rings is analyzed, as a function of the spherical coordinates ψ (circumferential angle) and θ (azimuthal angle) in Fig. 3. The maximum interference takes place in the contact point with coordinates ψ=θ=0, i.e. in the displacement line, with a value equal to the imposed radial displacement δ_0 as pointed out in Fig. 4.

Fig. 5a shows the interference field along the circumferential line (θ=0). The contact between rings occur in the range $-\psi_0<\psi<\psi_0$. Assuming small interferences in comparison with the diameter of the rings, the interference field has the following distribution [12]:

$$\delta(\psi) = \delta_0 \cdot \left(1 - \frac{1}{2 \cdot \varepsilon} \cdot (1 - cos\psi)\right) \tag{3}$$

In [12] it was supposed that the interference was constant in the azimuthal direction (thus approximating the real spherical contact surface by a cylindrical surface). In the present work the spherical surface is considered, with Fig. 5b showing the interference field along the azimuthal line (ψ=0). In this case contact occurs in the range $-\theta_0<\theta<\theta_0$, because the outer ring gets truncated at this angle (see Fig. 3). The interference has the same distribution as in the circumferential direction:

$$\delta(\theta) = \delta_0 \cdot \left(1 - \frac{1}{2 \cdot \varepsilon} \cdot (1 - cos\theta)\right) \tag{4}$$

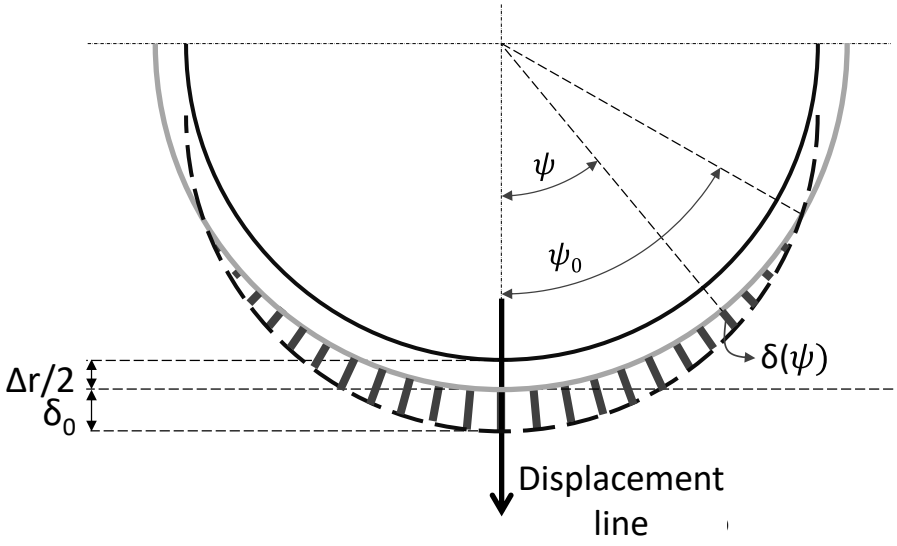

(a)

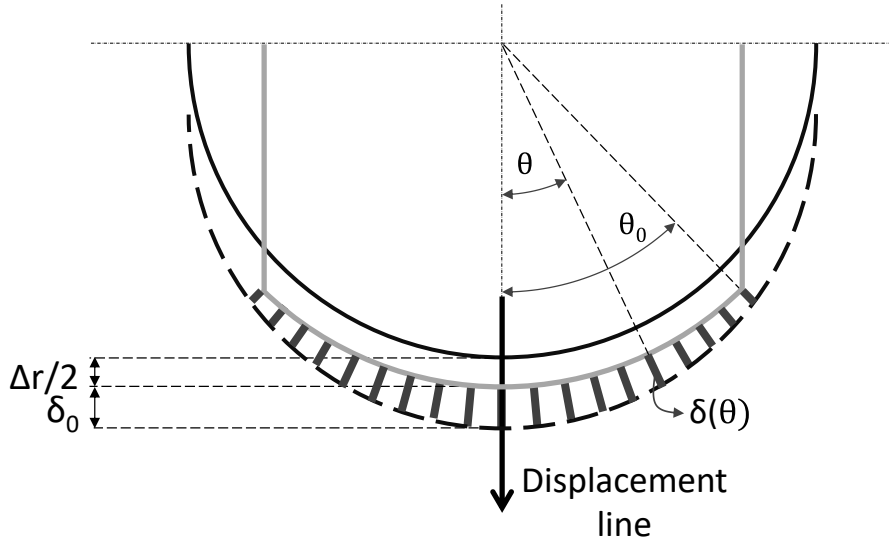

(b)

Fig. 5. Interference field under radial displacement: (a) along the circumferential line (θ=0) (b) along the azimuthal line (ψ=0).

Combining equations (3) and (4), the interference in any contact point (ψ,θ) is expressed as:

$$\delta(\psi,\theta) = \delta_0 \cdot \left(1 - \frac{1}{2 \cdot \varepsilon} \cdot (1 - cos\theta)\right) \cdot \left(1 - \frac{1}{2 \cdot \varepsilon} \cdot (1 - cos\psi)\right) \quad (5)$$

This interference field δ(ψ,θ) causes a pressure distribution p(ψ,θ) that, as postulated in [12], can be formulated in the following way:

$$p(\psi,\theta) = C \cdot \left(\delta(\psi,\theta)\right)^e \quad (6)$$

Where coefficients C and e are constants that must be calculated for each type of bearing by Finite Element Analyses, because their values depend on the geometry and materials. Equation (6) can be rewritten as:

$$p(\psi,\theta) = p_0 \cdot \left(1 - \frac{1}{2\cdot\varepsilon}\cdot(1-cos\theta)\right)^e \cdot \left(1 - \frac{1}{2\cdot\varepsilon}\cdot(1-cos\psi)\right)^e \quad (7)$$

Where p_0 is the pressure in the displacement line:

$$p_0 = C \cdot {\delta_0}^e \quad (8)$$

The radial component of the pressure field results in a radial load F_r that, according to Fig. 3, is calculated as:

$$F_r = \int p(\psi,\theta)\cdot cos\psi \cdot cos\theta \cdot dA \quad (9)$$

In spherical coordinates, the differential of area dA is:

$$dA = \left(\frac{d}{2}\right)^2 \cdot cos\theta \cdot d\theta \cdot d\psi \quad (10)$$

Substituting equations (7) and (10) in (9):

$$F_r = p_0 \cdot \left(\frac{d}{2}\right)^2 \cdot I \quad (11)$$

Being:

$$I = \iint \left(1 - \frac{1}{2\cdot\varepsilon}\cdot(1-cos\theta)\right)^e \cdot \left(1 - \frac{1}{2\cdot\varepsilon}\cdot(1-cos\psi)\right)^e \cdot cos\psi \cdot cos^2\theta \cdot d\theta \cdot d\psi \quad (12)$$

This surface integral is numerically solved. For instance, sweeping angles θ_i and ψ_j with one degree step size (π/180 rad) within the intervals $-90° < \theta_i < 90°$ and $-180° < \psi_j < 180°$, expression (12) is:

$$I = \left(\frac{\pi}{180}\right)^2 \cdot \sum\sum \left(\left(1 - \frac{1}{2\cdot\varepsilon}\cdot(1-cos\theta_i)\right)^e \cdot \left(1 - \frac{1}{2\cdot\varepsilon}\cdot(1-cos\psi_j)\right)^e \cdot cos\psi_j \cdot cos^2\theta_i\right) \quad (13)$$

Obviously, interference does not occur in all of the points of the spherical contact surface (see Fig. 5). If interference is negative in a (ψ_j,θ_i) point, no interference exists in that point, therefore the pressure is zero and the corresponding term in equation (13) must be considered null. This happens when the point (ψ_j,θ_i) fulfils any of the following conditions (deduced respectively form expressions (3) and (4), and from Fig. 5b):

$$1 - \frac{1}{2\cdot\varepsilon}\cdot(1-cos\psi_j) < 0 \quad (14a)$$

$$1 - \frac{1}{2\cdot\varepsilon}\cdot(1-cos\theta_i) < 0 \quad (14b)$$

$$abs(\theta_i) > \theta_0 \quad (14c)$$

Thus, using these expressions the radial force F_r caused by a radial interference δ_0 between the rings can be worked out.

2.2 Combined radial and axial load case

In this case, when the rings are in contact after having overcome the internal clearance Δr/2, the inner ring is displaced a distance δ_0 following a displacement line with an azimuthal angle θ=α as shown in Fig. 6; taking this line as a reference, new rotated spherical coordinates ψ´ and θ´ are defined. The displacement δ_0 will cause a radial load F_r and an axial load F_a, whose values want to be calculated.

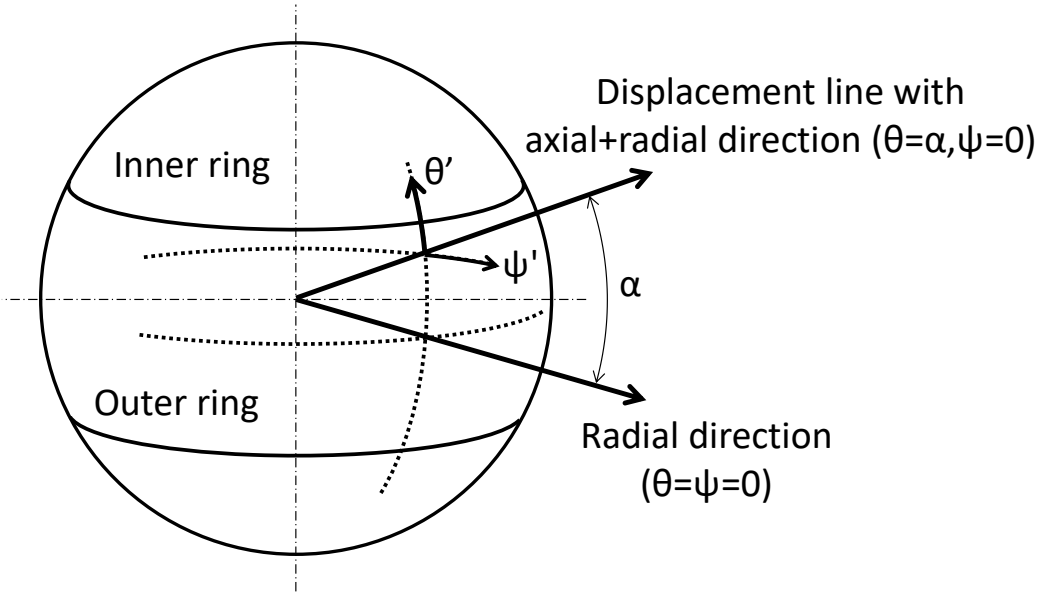

Fig. 6. Displacement line with radial + axial direction (θ=α, ψ=0).

The pressure distribution expressed as a function of the coordinates (ψ´,θ´) is analogous to the one presented in expression (7):

$$p(\psi',\theta') = p_0 \cdot \left(1 - \frac{1}{2\cdot\varepsilon}\cdot(1-cos\theta')\right)^e \cdot \left(1 - \frac{1}{2\cdot\varepsilon}\cdot(1-cos\psi')\right)^e \quad (15)$$

Loads F_r and F_a are calculated projecting the pressure field in radial and axial directions in the original coordinate system. From Fig. 6:

$$F_r = \int p(\psi',\theta')\cdot cos\psi \cdot cos\theta \cdot dA \quad (16a)$$

$$F_a = \int p(\psi',\theta')\cdot sin\theta \cdot dA \quad (16b)$$

Substituting (15) and (10) in (16a) and (16b):

$$F_r = p_0 \cdot \left(\frac{d}{2}\right)^2 \cdot I_r \quad (17a)$$

$$F_a = p_0 \cdot \left(\frac{d}{2}\right)^2 \cdot I_a \quad (17b)$$

Where:

$$I_r = \iint \left(1 - \frac{1}{2 \cdot \varepsilon} \cdot (1 - cos\theta')\right)^e \cdot \left(1 - \frac{1}{2 \cdot \varepsilon} \cdot (1 - cos\psi')\right)^e \cdot cos\psi \cdot cos^2\theta \cdot d\theta \cdot d\psi \quad (18a)$$

$$I_a = \iint \left(1 - \frac{1}{2 \cdot \varepsilon} \cdot (1 - cos\theta')\right)^e \cdot \left(1 - \frac{1}{2 \cdot \varepsilon} \cdot (1 - cos\psi')\right)^e \cdot cos\theta \cdot sin\theta \cdot d\theta \cdot d\psi \quad (18b)$$

Once again as in equation (13), integrals are numerically solved. As previously, sweeping angles θ_i and ψ_j with one degree step size ($\pi/180$ rad) within the intervals $-90° < \theta_i < 90°$ and $-180° < \psi_j < 180°$:

$$I_r = \left(\frac{\pi}{180}\right)^2 \cdot \sum\sum \left(\left(1 - \frac{1}{2 \cdot \varepsilon} \cdot (1 - cos\theta'_i)\right)^e \cdot \left(1 - \frac{1}{2 \cdot \varepsilon} \cdot (1 - cos\psi'_j)\right)^e \cdot cos\psi_j \cdot cos^2\theta_i\right) \quad (19a)$$

$$I_a = \left(\frac{\pi}{180}\right)^2 \cdot \sum\sum \left(\left(1 - \frac{1}{2 \cdot \varepsilon} \cdot (1 - cos\theta'_i)\right)^e \cdot \left(1 - \frac{1}{2 \cdot \varepsilon} \cdot (1 - cos\psi'_j)\right)^e \cdot cos\theta_i \cdot sin\theta_i\right) \quad (19b)$$

The values of $cos\theta'_i$ and $cos\psi'_j$ for each of the terms in expressions (19) can be calculated with the following equations, which relate the rotated spherical coordinates ψ' and θ' with the original coordinates ψ and θ:

$$sin\theta'_i = cos\theta_i \cdot cos\psi_j \cdot sin\alpha + sin\theta_i \cdot cos\alpha \quad \rightarrow \quad cos\theta'_i = \sqrt{1 - sin^2\theta'_i} \quad (20a)$$

$$cos\psi'_J = \frac{cos\theta_i \cdot cos\psi_j - sin\theta'_i \cdot sin\alpha}{cos\theta'_i \cdot cos\alpha} \quad (20b)$$

Points (ψ_j,θ_i) with negative interference have a null pressure and their corresponding term in equations (19) must be zero. As in equations (14), this occurs when any of the following conditions are met:

$$1 - \frac{1}{2 \cdot \varepsilon} \cdot \left(1 - cos\psi'_j\right) < 0 \quad (21a)$$

$$1 - \frac{1}{2 \cdot \varepsilon} \cdot (1 - cos\theta'_i) < 0 \quad (21b)$$

$$\text{abs}(\theta_i) > \theta_0 \quad (21c)$$

3. Calculation of load magnification factors

By means of the procedure and expressions described in the previous section, starting from a displacement δ_0 of the inner ring with respect to the outer ring, the proposed model calculates the contact interferences and pressures, and the corresponding F_a and F_r that originate them. The larger the displacement δ_0, the larger the pressures and loads. As explained in the Introduction section, the failure takes place when the maximum contact pressure reaches a design limiting value p_{max}. This pressure occurs in the point where the interference is maximum (δ_{max}), with the following value according to equation (6):

$$\delta_{max} = \left(\frac{p_{max}}{C}\right)^{1/e} \quad (22)$$

The point with maximum interference δ_{max} is not always the same: if $\alpha<\theta_0$ as in Fig. 7a, δ_{max} occurs in the displacement line with a value $\delta_{max}=\delta_0$; if $\alpha>\theta_0$ as in Fig. 7b, there is no contact in the displacement line and the maximum interference δ_{max} occurs in the angle $\theta=\theta_0$, being its value lower than δ_0. Thus:

$$\text{if } \alpha < \theta_0 \rightarrow \delta_0 = \delta_{max} \tag{23a}$$

$$\text{if } \alpha > \theta_0 \rightarrow \delta_0 = \frac{\delta_{max}}{\left(1-\frac{1}{2\cdot\varepsilon}\cdot(1-cos(\theta_0-\alpha))\right)} \tag{23b}$$

Consequently, as δ_0 is different for $\alpha<\theta_0$ and $\alpha>\theta_0$, the value of ε will also be different in each case. Substituting expressions (23) in (2):

$$\text{if } \alpha < \theta_0 \rightarrow \varepsilon = \frac{\delta_{max}}{\Delta r+2\cdot\delta_{max}} \tag{24a}$$

$$\text{if } \alpha > \theta_0 \rightarrow \varepsilon = \frac{\frac{1}{\left(1-\frac{1}{2\cdot\varepsilon}\cdot(1-cos(\theta_0-\alpha))\right)}}{\frac{\Delta r}{\delta_{max}}+2\cdot\frac{1}{\left(1-\frac{1}{2\cdot\varepsilon}\cdot(1-cos(\theta_0-\alpha))\right)}} \tag{24b}$$

Note that equation (24b) must be solved iteratively to calculate ε.

To sum up, from displacements δ_0 in expressions (23a) or (23b) depending on the value of α, the method calculates the loads F_r and F_a that cause the limit pressure p_{max} and therefore the failure of the bearing. In this sense, curves F_a/F_r-Y like the ones presented in Fig. 2 are obtained following the steps listed in the flowchart in Fig. 8.

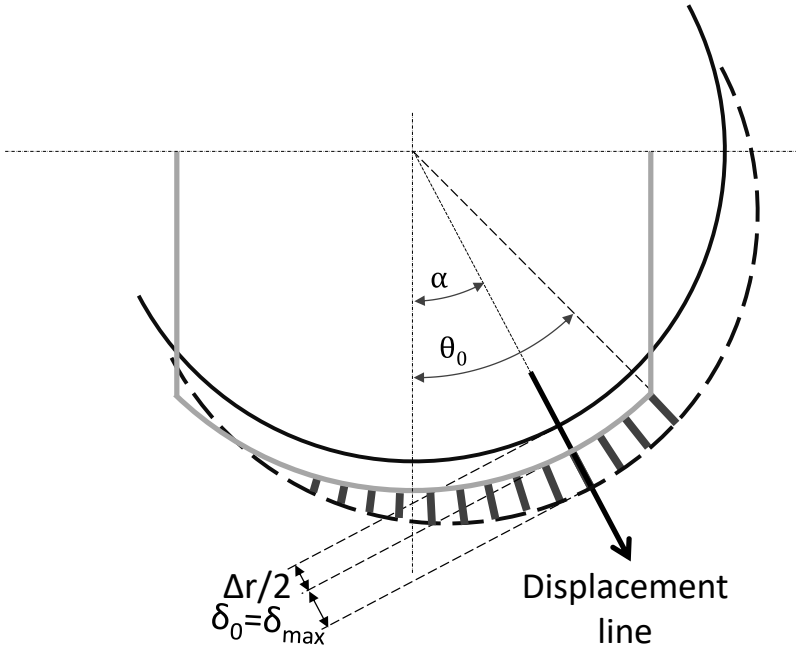

(a)

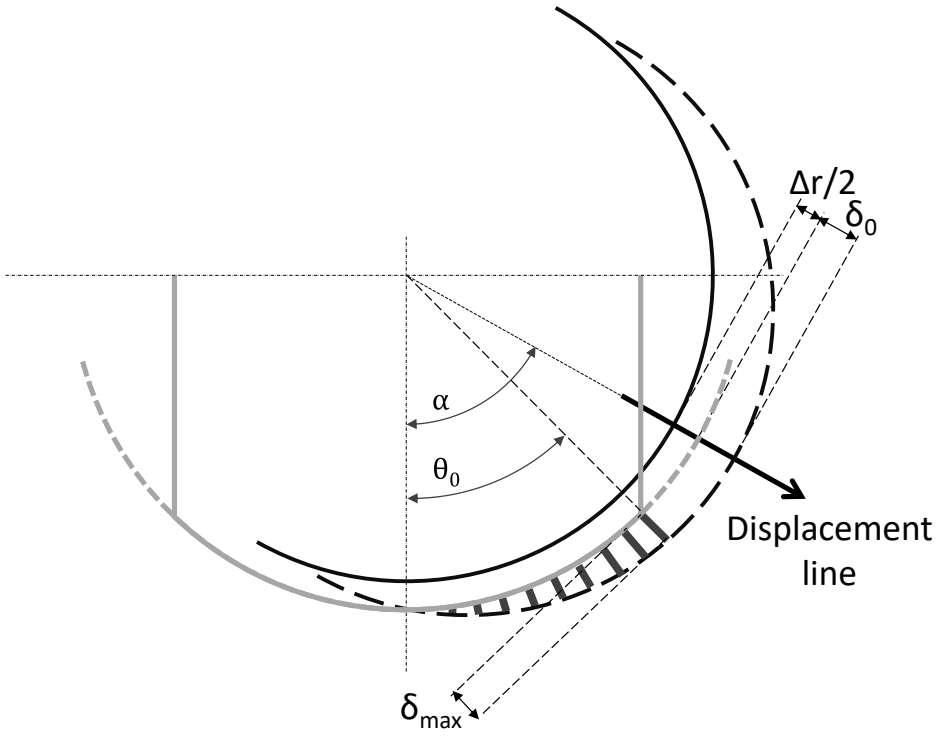

(b)

Fig. 7. Interference field: (a) $\alpha<\theta_0$: $\delta_0=\delta_{max}$ (b) $\alpha>\theta_0$: $\delta_0\neq\delta_{max}$.

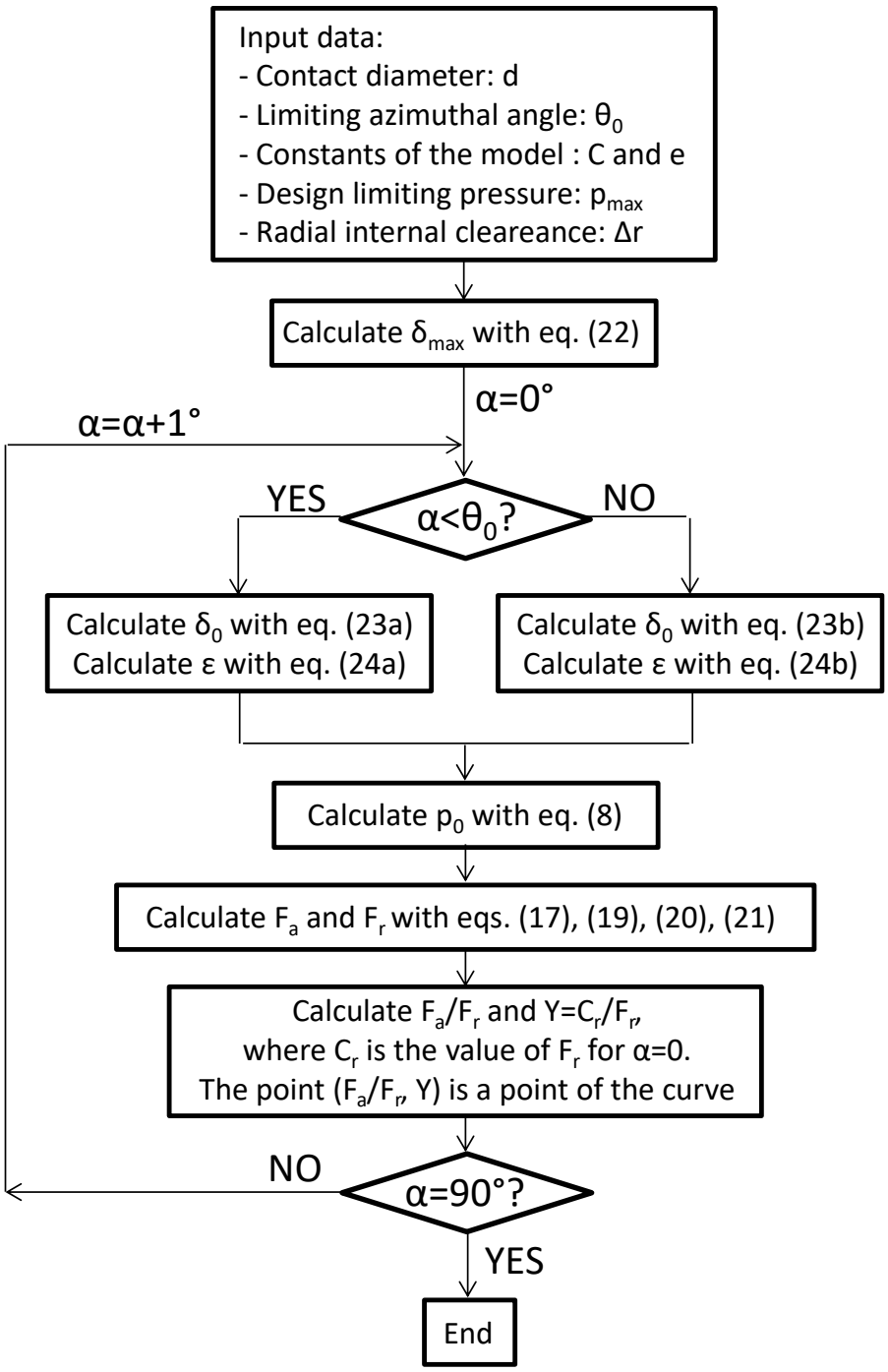

Fig. 8. Flowchart for the calculation of the load magnification factors using the proposed model.

4. Results and discussion

As it has been pointed out in the Introduction section, Fig. 2 shows the load magnification factors provided by manufacturer SKF for the self-lubricating radial spherical plain bearings: one curve is for series GEP..FS and the other one for the rest of the series. Following the flowchart of Fig. 8, the proposed model has been used to calculate the same factors; in order to validate the proposed model, the curves obtained and the ones by SKF must be similar.

Fig. 8 shows that the input data for the proposed model are the contact diameter d, the limiting azimuthal angle θ_0, the constants C and e, the design limiting pressure p_{max} and the clearance Δr. Bearing GEP 320 FS from series GEP..FS and bearing GEC 320 TXA-2RS from the other series have been selected as representative of each type [3].

Contact diameter d, angle θ_0 and clearance Δr are extracted from the catalogue, with the values listed in Table 1. The limiting pressure p_{max} is a design parameter chosen by the manufacturer depending on the features of its particular products. Introducing for each bearing a pure radial load equal to the radial static load capacity (whose value is pointed out in the catalogue) in the proposed model, the maximum contact pressure is approximately 300MPa for bearing GEP 320 FS and 1000MPa for bearing GEC 320 TXA-2RS so, in the absence of more accurate data from the manufacturer, these are the values adopted for p_{max} (see Table 1). These values are probably different from those used by SKF in practice, and different from the ones used by other manufacturers; in any case, for the new methodology presented in this work this is just an input parameter to be provided by the manufacturer, so it does not compromise its validity and applicability.

Finally, as it was mentioned when equation (6) was presented, the values for constants C and e depend on the geometry and materials of the bearing. The values have been calculated by means of Finite Element models like the one shown in Fig. 9: the model consists of half bearing taking advantage of the symmetry of the system, with the exterior face of the outer ring clamped, the symmetry plane with its out-of-plane movements restricted, and with more than 600000 degrees of freedom. A progressively increasing radial displacement δ_0 has been imposed to the inner face of the inner ring and the resulting pressure distribution has been compared with the one predicted by expressions (7) and (8) to obtain the values for parameters C and e. As listed in Table 1, for bearing GEC 320 TXA-2RS the values are C=4333 and e=1 (with pressure measured in MPa and interference in mm); it has been verified that these values do not depend on the load magnitude and the clearance Δr of the bearing. For bearing GEP 320 FS the values are C=3825 and e=1 (see Table 1), but only when the clearance is null ($\Delta r=0$); it has been observed that for minimum and maximum clearances indicated in Table 1, the pressure does not have the distribution predicted by equation (6), and therefore the proposed model does not fit properly these cases. The authors believe that this limitation is due to the differential features of series GEP..FS bearing, which have larger contact angles and smaller contact pressures than the other series. Nevertheless, the proposed model works correctly for null clearance, so the load magnification factors have been obtained with the values of C and e obtained for this case (see Table 1).

Fig. 10 shows, together with the curves by SKF previously shown in Fig. 2, the load magnification factors obtained with the proposed model following the steps in the flowchart of Fig. 8; for bearing GEP 320 FS only the curve with null clearance is shown as justified.

The curves obtained by FE models for both bearings are also illustrated. For such purpose, once again the inner face of the inner ring is increasingly displaced (as it was done to calculate C and e), in this case until the maximum pressure contact reaches p_{max}. When that occurs, the axial (F_a) and radial (F_r) reactions in the clamped outer ring, which will be a failure load combination, are computed; the load magnification factor Y for that F_a/F_r value can be then easily calculated by dividing C_r by F_r according to equation (1), and thus a (F_a/F_r,Y) point of the curve is obtained. Different points are obtained by varying the direction of the displacement applied to the inner ring.

As explained before, the FE model assumes rigid boundary conditions; however, in practice shafts and supports attached to the bearing are flexible. Contact pressure distribution will be affected by the boundary conditions, so this assumption introduces an error in the values of Y [11,16-17]. However, as each application has its own particular boundary conditions, and since the aim of this work is to develop a generalist method, the use rigid boundary conditions is considered appropriate.

The FE results confirm the validity of the proposed model: the slight difference between the results is due to the existence of pressure concentrations in the edges of the contact surface near the azimuthal angle θ_0 (see Fig. 3), which the proposed model does not consider: Figures in Table 2 shows the pressure distribution in bearing GEC 320 TXA-2RS for different analyses, illustrating this free-edge effect; Figure 11 compares the pressure distributions of the FE model and the proposed model for a certain load case (GEC 320 TXA-2RS, Δr=100μm, α=60° shown in Table 2), further illustrating this phenomenon. Besides, it can be observed in Fig. 10 that the results of the proposed model are similar to the ones given by SKF. In this sense, the model proposed in this work can be used for any manufacturer to compute its own load magnification factors for its particular products and design parameters.

It must be emphasized that the shape of the curves does not depend on the value of the radial capacity C_r of the bearing, because the load magnification factor Y is normalized with respect to C_r according to equation (1). In other words, the curves are the same regardless of the capacity value adopted by the manufacturer.

Table 1. Input data for the proposed model for the bearings under study.

	GEC 320 TXA-2RS	**GEP 320 FS**
d (mm)	380	414
θ_0 (°)	15.45	31.77
Δr min (μm)	100	135
Δr max (μm)	230	490
p_{max} (MPa)	1000	300
C	4333	3825*
e	1	1*

*Values for null clearance case. No null clearance cases do not fit properly equation (6).

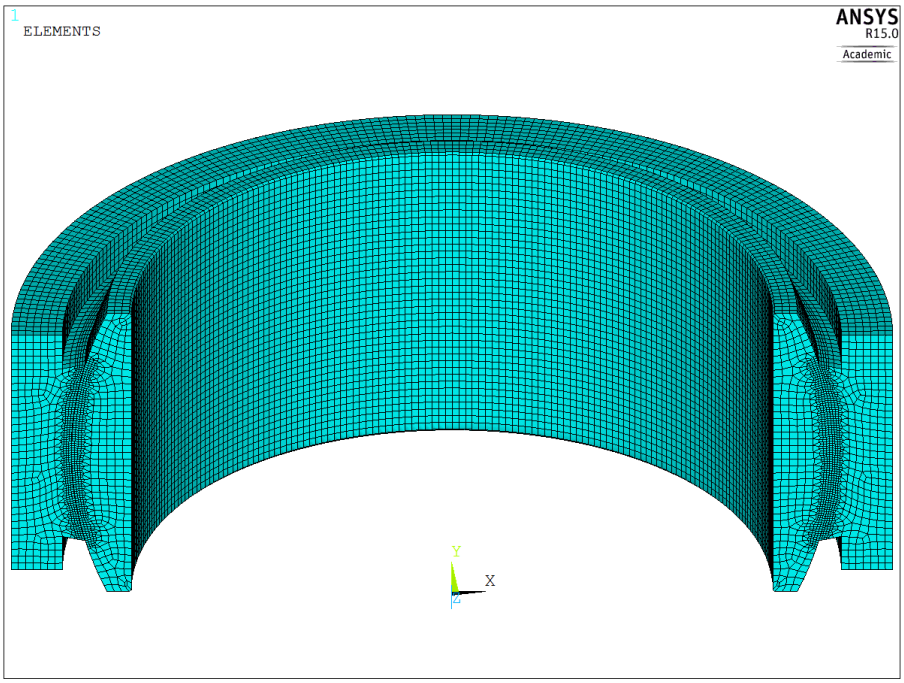

Fig. 9. Finite Element model of the bearing GEC 320 TXA-2RS.

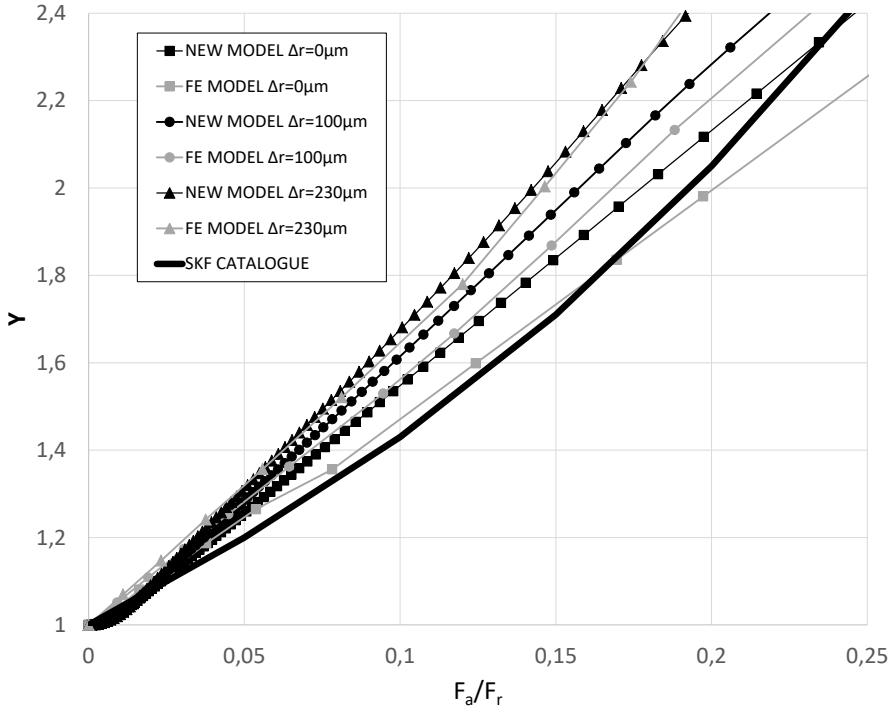

(a)

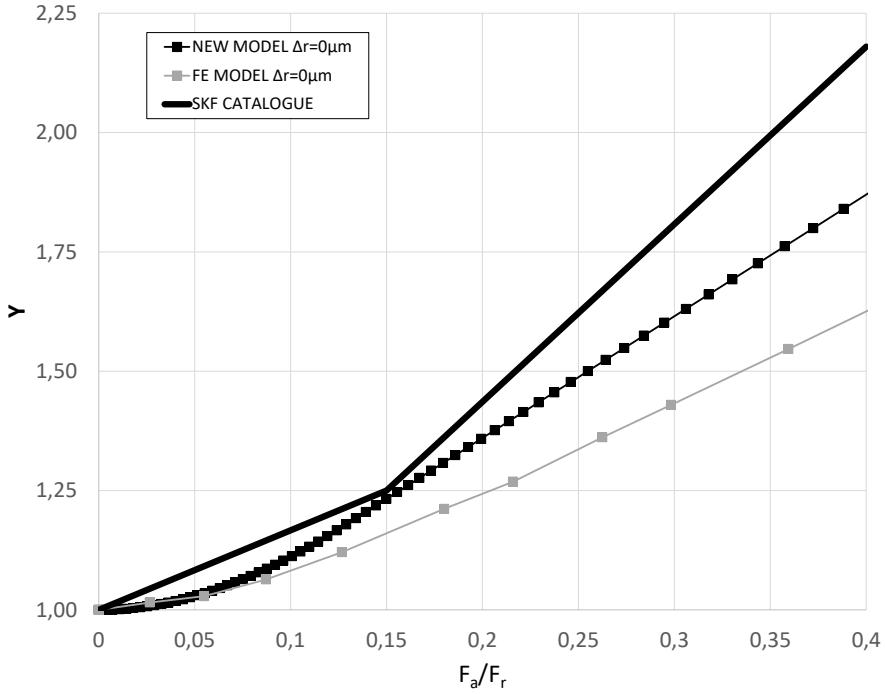

(b)

Fig. 10. Fa/Fr-Y curves: (a) bearing GEC 320 TXA-2RS (b) bearing GEP 320 FS

Table 2. Pressure distribution of FE model of bearing GEC 320 TXA-2RS for different analyses.

Δr=100μm	**Δr=230μm**
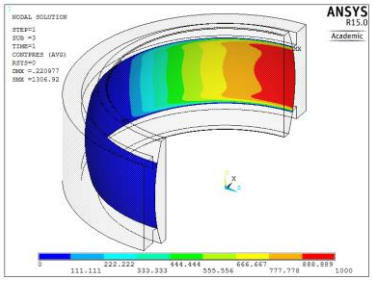	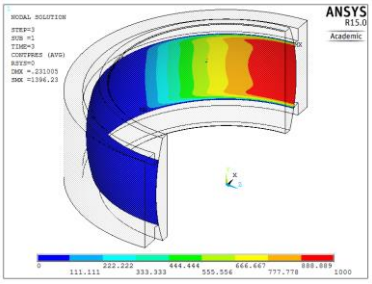
α=0°; Fa/Fr=0	α=0°; Fa/Fr=0
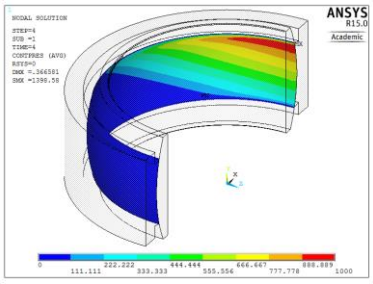	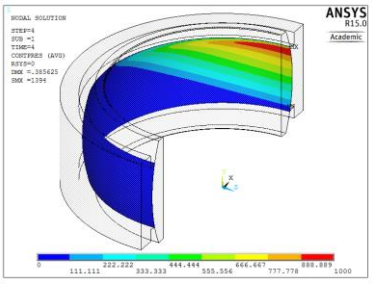
α=60°; Fa/Fr=0.095	α=60°; Fa/Fr=0.120

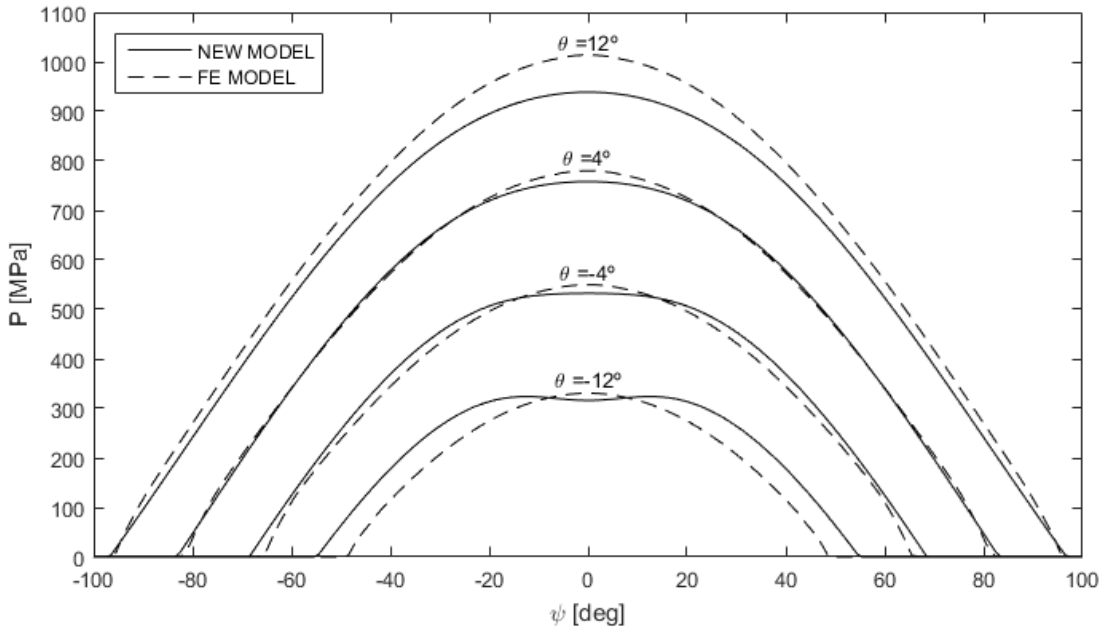

(a)

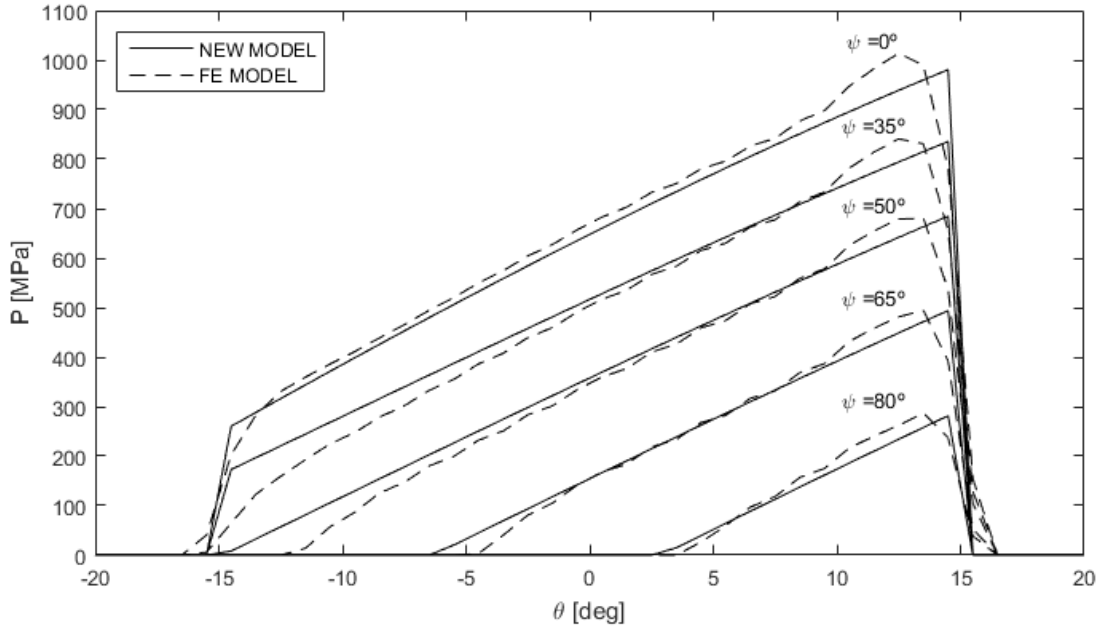

(b)

Fig. 11. Pressure distribution curves (for different θ and ψ values) for bearing GEC 320 TXA-2RS, Δr=100μm, α=60°

5. Conclusions

The calculation of the load magnification factors for equivalent radial load in self-lubricating radial spherical plain bearings is not published in any standard yet. The

manufacturers explain how to calculate the radial load capacity, which must be larger than the acting radial load to avoid failure. Nevertheless, radial spherical plain bearings can carry radial and axial combined loads; for these load cases, manufacturers provide some load magnification factors whose background is not explained anywhere.

The present work proposes a model which studies the interference field and therefore the pressure distribution in the contact surface. As a direct application, an algorithm has been developed to obtain the magnification factors. The factors obtained by the proposed model, which have been validated via Finite Element Analysis, are similar to the ones provided by manufacturer SKF. Thus, this work fills a gap in the literature of the calculation of the load magnification factor of self-lubricating radial spherical plain bearings, presenting an original model that can be used by any manufacturer to obtain their own load magnification factors for their products.

Acknowledgements

The authors wish to acknowledge the financial support of the Spanish Ministry of Economy and Competitiveness (MINECO) through Grant Number DPI2013-41091-R and the University of the Basque Country (UPV/EHU) through Grant Number UFI11/29. This work is a result of the close collaboration that the authors maintain with the bearing manufacturer Iraundi.

Conflict of interest

The authors declare that they have no conflict of interest.

References

[1] International Standard ISO 12240-1:1998. Spherical plain bearings-Part 1: Radial spherical plain bearings.

[2] American Standard ANSI/ABMA Std. 22.2-1988. Spherical Plain Radial Bearings, Joint-type - Inch Design.

[3] SKF website: http://www.skf.com/mena/products/bearings-units-housings/plain-bearings/general/selection-and-application/selecting-bearing-size/loads/equivalent-static-load/index.html.

[4] Hertz H. On the contact of elastic solids. *J Reine Angew Math* 1882; 92;156-171.

[5] Johnson KL. Contact Mechanics. 2nd Edition. New York. Cambridge University Press; 1985.

[6] Sun Z, Hao C. Conformal contact problems of ball-socket and ball. *Physics Procedia* 2012; 25:209-214.

[7] Steuermann E. To Hertz´s theory of local deformation of compressed bodies. Comptes Rendus de l´Academie des Sciences de l´URSS 1939; 25:359-361.

[8] Goodman LE, Keer LM. The contact stress problem for an elastic sphere indenting an elastic cavity. *International Journal of Solids and Structures* 1965; 1 (4):407-415.

[9] Fagan M, McConnachie J. A review and detailed examination of non-layered conformal contact by finite element analysis. *The Journal of Strain Analysis for Engineering Design* 2001; 36(2):177-195.
[10] Fang X, Zhang C, Chen X, Wang Y, Tan Y. A new universal approximate model for conformal contact and non-conformal contact of spherical surfaces. *Acta Mechanica* 2015; 226 (6): 1657-1672.
[11] Fang X, Zhang C, Chen X, Wang Y, Tan Y. Newly developed theoretical solution and numerical model for conformal contact pressure distribution and free-edge effect in spherical plain bearings. *Tribology International* 2015; 84: 48–60.
[12] Laszlofalvi Z, Schutz KH. Maximum specific bearing load in maintenance-free plain bearings (Part I). *Ball Bearing Journal* 1981; 209:1-6.
[13] Laszlofalvi Z, Schutz KH. Maximum specific bearing load in maintenance-free plain bearings (Part II). *Ball Bearing Journal* 1982; 211:9-16.
[14] Aguirrebeitia J, Plaza J, Abasolo M, et al. General static load-carrying capacity of four-contact-point slewing bearings for wind turbine generator actuation systems. *Wind Energy* 2012; 16: 759–774.
[15] Pinedo B, Aguirrebeitia J, Conte M, Igartua A. Tri-dimensional eccentricity model of a rod lip seal. *Tribology International* 2014; 78: 68–74.
[16] Germaneau A, Peyruseigt F, Mistou S, Doumalin P, Dupré JC. 3D mechanical analysis of aeronautical plain bearings: validation of a finite element model from measurement of displacement fields by digital volume correlation and optical scanning tomography. *Optics and Lasers in Engineering* 2010; 48(6): 676–83.
[17] Plaza J, Abasolo M, Coria I, Aguirrebeitia J. A new finite element approach for the analysis of slewing bearings in wind turbine generators using superelement techniques. *Meccanica* 2015; 50(6): 1623–1633.